Supplemental Information

KAT–independent gene regulation by Tip60 promotes ESC self-renewal but not pluripotency

Diwash Acharya, Sarah J. Hainer, Yeonsoo Yoon, Feng Wang, Ingolf Bach, Jaime A. Rivera-Pérez, and Thomas G. Fazzio

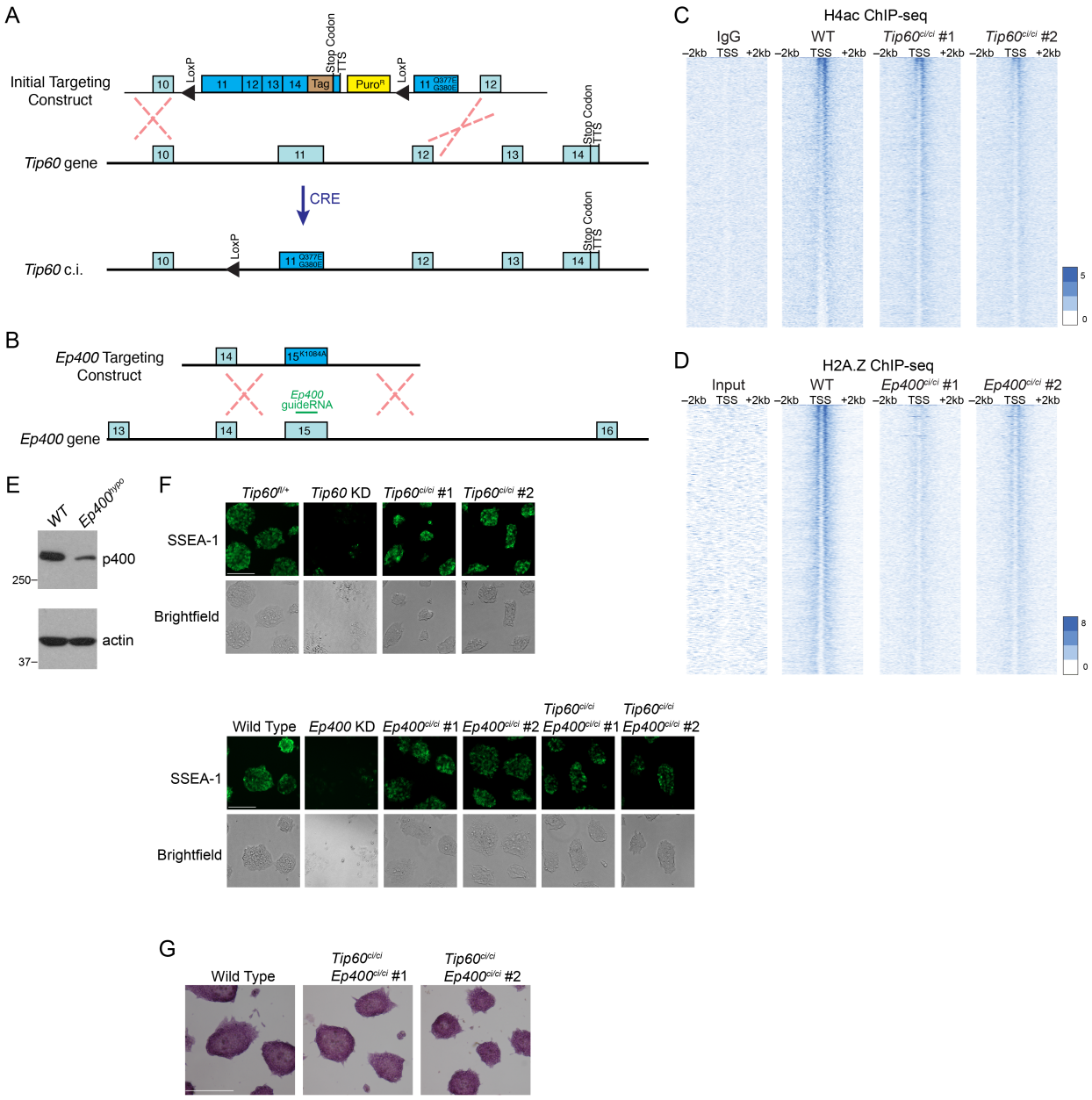

Figure S1. Generation and phenotypes of *Tip60*$^{ci/ci}$ and *Ep400*$^{ci/ci}$ mutants, Related to Figure 1. (**A**) Schematic representation of *Tip60*$^{ci/ci}$ lines generated using homologous recombination of the construct, followed by Cre-LoxP–mediated excision of the wild type *Tip60* sequence. (**B**) Schematic for generation of *Ep400*$^{ci/ci}$ mutants using CRISPR/Cas9 mediated homologous recombination. (**C**) ChIP-seq of tetra-acetylated H4 (K5/8/12/16) in wild type and two *Tip60*$^{ci/ci}$ lines. Heatmaps are over TSS-proximal regions (+/- 2kb), sorted from highest H4ac to lowest. IgG is a specificity control. (**D**) H2A.Z ChIP-seq in wild type or two *Ep400*$^{ci/ci}$ mutant ESC lines, as in (**C**). (**E**) Western blot confirmation of *Ep400*^{hypo} lines, generated using CRISPR/Cas9 without the repair template. (**F**) SSEA-1 live cell staining of *Tip60*$^{ci/ci}$, *Ep400*$^{ci/ci}$, and *Tip60*$^{ci/ci}$*Ep400*$^{ci/ci}$ mutants, compared to their respective controls *Tip60*$^{fl/+}$, *Tip60* KD, Wild Type and *Ep400* KD. (**G**) AP staining of *Tip60*$^{ci/ci}$*Ep400*$^{ci/ci}$ mutants as in Figure 1A. Scale bars equal 200 mm in both (**F**) and (**G**).

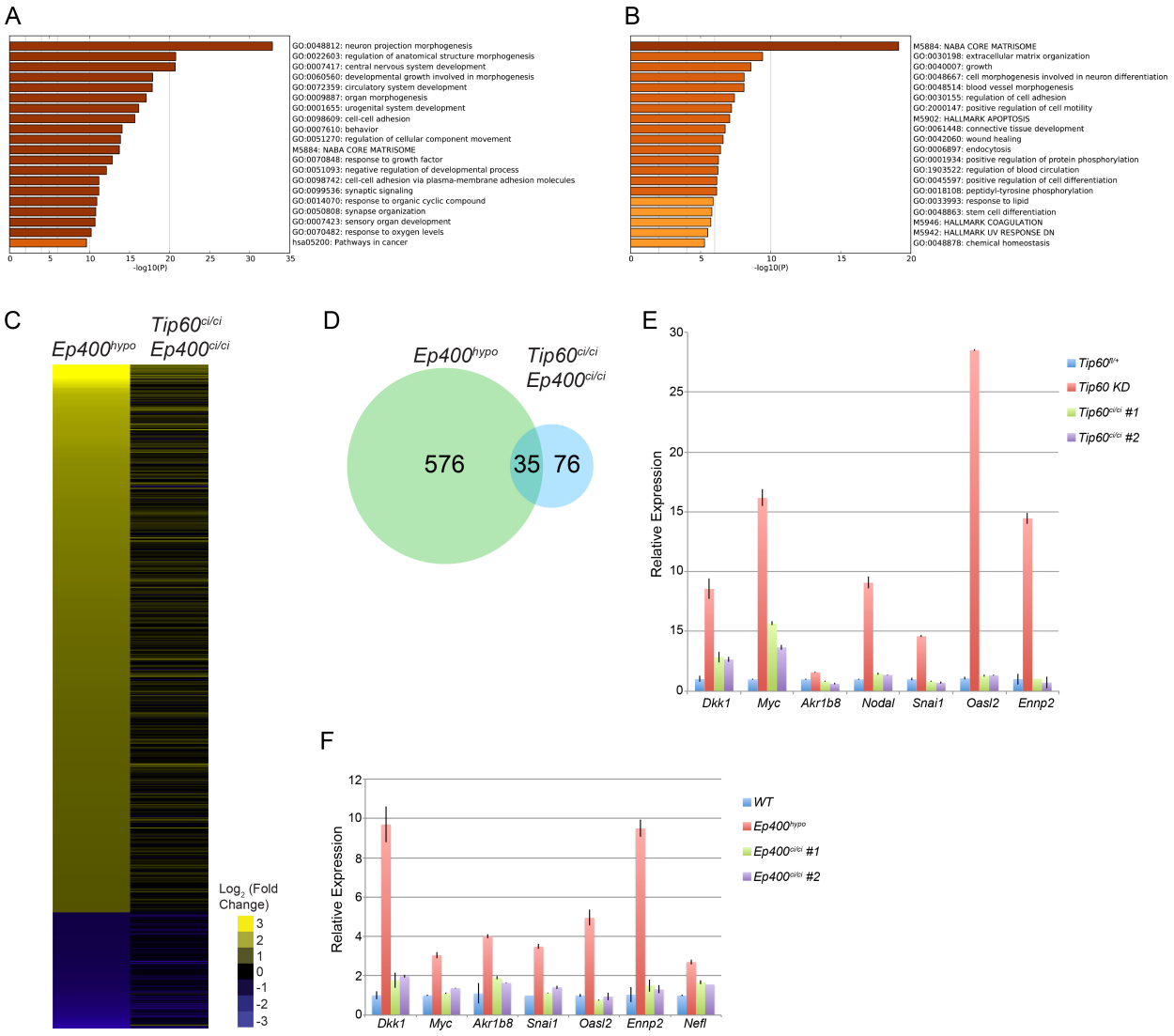

Figure S2. Catalytic activity-independent gene regulation by Tip60-p400, Related to Figure 1. (**A, B**) GO (Gene ontology) terms enriched within genes upregulated in *Tip60* KD (**A**), and *Ep400*^{hypo} ESCs (**B**), as measured by RNAseq. Shown are histograms depicting the significance (-log$_{10}$ p value) of GO categories enriched in each gene set (generated by Metascape; http://metascape.org). (**C**) Heatmaps of differentially expressed genes in *Tip60*$^{ci/ci}$ *Ep400*$^{ci/ci}$ ESCs relative to *Ep400*^{hypo} control cells, as in Figure 1. (**D**) Venn diagram showing number of significantly misregulated genes commonly misregulated in *Tip60*$^{ci/ci}$*Ep400*$^{ci/ci}$ and *Ep400*^{hypo} ESCs, as in Figure 1. (**E, F**) RT-qPCR measuring mRNA levels of Tip60-p400 target genes in mutants or control ESCs as indicated. mRNA levels were normalized to *GAPDH*.

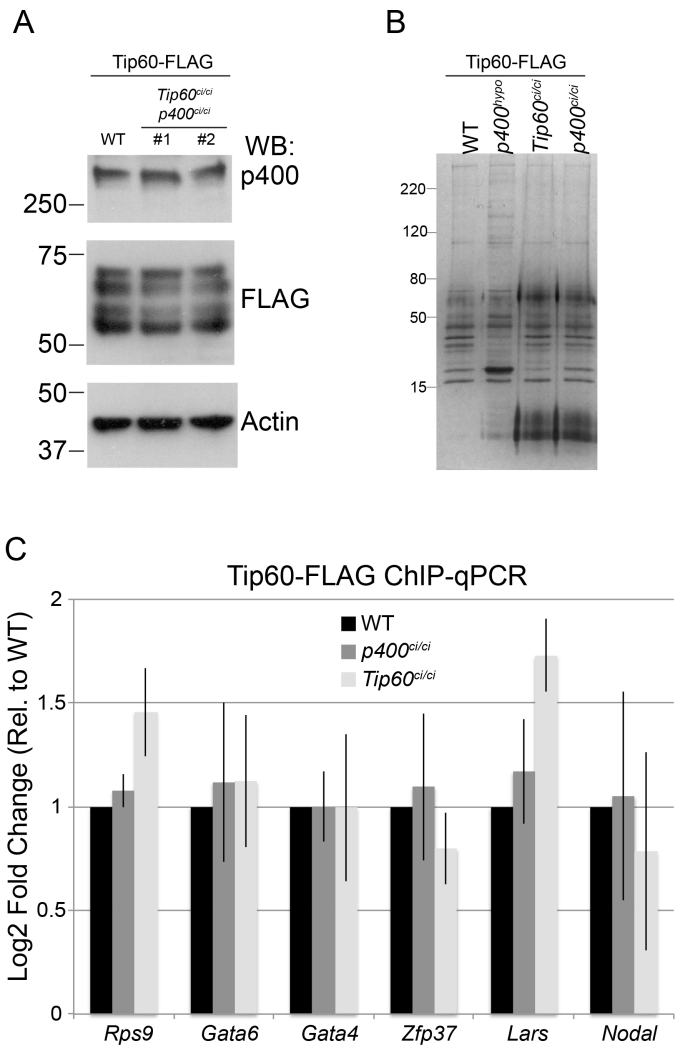

Figure S3. Catalytically inactive Tip60-p400 mutations do not compromise complex integrity, Related to Figure 2. (**A**) Western blots indicating equal expression of catalytic subunits of Tip60-p400 in wild type or double catalytically inactive mutant ESCs. Actin is a loading control. (**B**) Silver stain of Tip60-p400 complex purified from lines with genotypes indicated at top. In each case, Tip60 is FLAG-tagged at both copies of its endogenous locus. (**C**) Tip60-FLAG ChIP-qPCR from WT, *Tip60*$^{ci/ci}$, and *Ep400*$^{ci/ci}$ ESCs show similar Tip60 occupancy in each. Shown are biological triplicate ChIP-qPCRs from each line, normalized to untagged control ESCs, and expressed relative to WT.

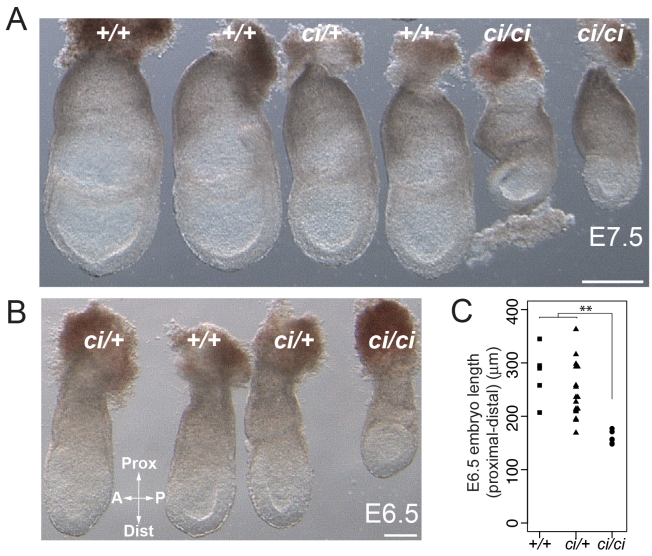

Figure S4. Phenotypes of *Tip60*$^{ci/ci}$ embryos, Related to Figure 3. (**A, B**) Brightfield images of E7.5 and E6.5 embryos from *Tip60*$^{ci/ci}$ intercrosses, with their genotypes (determined after imaging) indicated. Scale bars equal 100 mm. (**C**) Measurement of the length of the proximal distal axis of embryos (epiblast + extraembryonic endoderm) of the indicated genotypes (**p < 0.01, calculated using a two sided t-test).

Table S1. RTqPCR primers, Related to Figure 3.

Nestin	Forward: TGGCACACCTCAAGATGTCCCTTA Reverse: AAGGAAATGCAGCTTCAGCTTGGG
Sox11	Forward: ACGACCTCATGTTCGACCTGAGCT Reverse: CACCAGCGACAGGGACAGGTTC
T	Forward: CCAAGGACAGAGAGACGGCT Reverse: AGTAGGCATGTTCCAAGGGC
Flk1	Forward: GCTTGCTCCTTCCTCATCTC Reverse: CCATCAGGAAGCCACAAAGC
Sox17	Forward: CTCGGGGATGTAAAGGTGAA Reverse: GCTTCTCTGCCAAGGTCAAC
FoxA2	Forward: CCCTACGCCAACATGAACTCG Reverse: GTTCTGCCGGTAGAAAGGGA
Dkk1	Forward: ACTCAAATGGCTTTGGTAATATGG Reverse: ATAATCTCTTCTGAATTCTGCCCA
Myc	Forward: AGCTGTTTGAAGGCTGGATTTC Reverse: GCAACATAGGATGGAGAGCAGA
Akr1b8	Forward: TACTGTCACTCGAAGGGCATCT Reverse: ATCTCCTCGTCACTCAACTGGA
Nodal	Forward: TCCTTCTTCTTCAAGCCTGTTG Reverse: CCAGATCCTCTTCTTGGCTCA
Snai1	Forward: CTTGTGTCTGCACGACCTGTG Reverse: AGACTCTTGGTGCTTGTGGAG
Oasl2	Forward: TTGTGCGGAGGATCAGGTACT Reverse: TGATGGTGTCGCAGTCTTTGA
Ennp2	Forward: ATGGCAAGACAAGGCTGTTTC Reverse: TTGACGCCGATGGCAAAAGT
Scamp1	Forward: CCTTGAGGTCTGTGGTATTGGA Reverse: TACACCCTTAGTGACCTCAGTGTC
Nefl	Forward: AGCTAGAGGACAAGCAGAATGC Reverse: GCAAGCCACTGTAAGCAGAAC

Supplemental Table S2. Genotyping primers, related to Figure 3.

Tip60$^{ci/+}$ or *Tip60*$^{ci/ci}$ (mice and ESCs)	Forward: GTGGGCTACTTCTCCAAGGTC Reverse: TGTGAAGCACAGATGAGGGT

Supplemental Table S3. *Ep400* repair template, related to Figures S1-S3 and Figure 1.

(**K1084A mutation**; silent PAM mutation; *guideRNA sequence*)
TAGGCTCATAAAACTCACAGCAGTCTGAGTTGTGTCTATTTCATTGTTGTTGTAGATGTAGAAGACTG TCCTAGTGACAGGGAGAGCCGGAGGGACTCCGTTCTCATTGACTCACTCTTCATCATGGATCAGTTT AAAGCTGCAGAGAGAATGAGCATTGGAAAATCCAACACCAAGGACATCACAGAAGTTACTGCTGTGG CTGAAGCCATCCTCCCTAAGGGCAGTGCCCGAGTCACAACTGCGGTGAGGAAAGCCTTTCCTGCCT CCCAAACACGCTCCATAGGAATGCCTAGAAAAGGCAGTTCTTGTGTCCTTATGTTCTGTAAATCATTT GGGATAGTCTCTCGATTTAGGCTCTGAGAAGGTGTGTGCCAATTACTCACTCTTTGGCTGGTCTGTC TGTCTCTATAGGTGAAGTTTAGTGCTCCATCTTTGTTGTATGGTGCTCTCCGAGACTATCAGAAGATA GGCCTGGACTGGTTGGCCAAGCTATACCGGAAGAATCTCAATGGCATAT*TGGCTGATGAAGCAGGG* *CTT*GGC**GCC**ACTGTGCAGATCATTGCTTTTTTTGCTCACCTTGCCTGTAATGAAGGTAAGATCCTCTC AGTCTCCACTAAGAGCGTGTGTTAGATCTGAGAGAAAAGAAATTGTCAGCCTCTTTTGCTCATCTCTC TTTCTTGAGCCAAGAAATGACTCTCCTTTTTAAAATTTTTATTTATTTTTTTATTCTTTGCATACATTATA TCTCGACCACACCATTCTTCCCAGAGTCTTCCTCCATCATCTTCTCCCCAGGAGCTTCCATTACCATA AAAAAATAAAACCAACAAATAACAGCAACAAAAAACAAAAAGCAGGCATCCCAGGGATATCCACCATA CATGGCATAACAAGTTACAGTGAGACTAGGCACAAACCCTCATCTCAAGGCTGGATGAGGCAGCCC AGTAGA

Supplemental Methods

Deep sequencing data analysis

RNA-seq

TopHat2 (Kim et al., 2013) was used to map the RNAseq reads to the mouse genome (mm10) using parameters (--library-type fr-firststrand --segment-length 38). The bam files from the Tophat output were used for downstream analysis using HOMER (Heinz et al., 2010). DESeq2 (Love et al., 2014) was used to identify the differentially expressed genes. Heatmaps were generated using Java TreeView (Saldanha, 2004). K-means clustering was performed using Cluster 3.0 (de Hoon et al., 2004), and GO term enrichment was calculated using Metascape software (http://metascape.org) (Tripathi et al., 2015).

ATAC-seq

Paired-end 75 bp reads were trimmed to 24 bases and reads were then aligned to mm10 using Bowtie2 with the parameter -X 2000 to ensure that fragments up to 2 kb were allowed to align. Duplicates were then removed using Picard (http://broadinstitute.github.io/picard/). Reads with low quality score (MAPQ < 10) and reads mapping to the mitochondrial genome (chrM) were removed. Reads were separated into size classes as described (Buenrostro et al., 2013) and only nucleosome free reads (less than 100 bp) were used for subsequent analyses. These reads were processed in HOMER (Heinz et al., 2010). Genome browser tracks were generated from mapped reads using the "makeUCSCfile" command. Mapped reads were aligned over specific regions using the "annotatePeaks" command to make 20 bp bins over regions of interest and sum the reads within each bin. Experiments were aligned over high quality (peak score > 6) Tip60 peaks called from (Ravens et al., 2015), that were subsequently separated into

promoter-proximal and –distal groups. After anchoring mapped reads over reference sites, aggregation plots were generated by averaging data obtained from biological replicates. Heatmaps were ordered based on clustering of reads summed over -100 bp to +100 bp from the Tip60 peak center through K-means clustering using Cluster 3.0.

ChIP-seq

Single-end raw FastQ reads were collapsed, adaptor sequence were removed, and reads were mapped to the mouse mm10 genome using bowtie, allowing one mismatch. Aligned reads were used for downstream analysis using the "annotatePeaks" command in HOMER (Heinz et al., 2010) to make 20 bp bins over promoter proximal regions and summing the reads within each bin. Experiments were aligned over high quality (peak score > 6) promoter-proximal Tip60 peaks called from (Ravens et al., 2015). After anchoring mapped reads over the reference site, heatmaps for biological replicates were generated using Java Treeview.

Supplemental References

Buenrostro, J.D., Giresi, P.G., Zaba, L.C., Chang, H.Y., Greenleaf, W.J., 2013. Transposition of native chromatin for fast and sensitive epigenomic profiling of open chromatin, DNA-binding proteins and nucleosome position. Nat Meth 10, 1213–1218. doi:10.1038/nmeth.2688

de Hoon, M.J.L., Imoto, S., Nolan, J., Miyano, S., 2004. Open source clustering software. Bioinformatics 20, 1453–1454. doi:10.1093/bioinformatics/bth078

Heinz, S., Benner, C., Spann, N., Bertolino, E., Lin, Y.C., Laslo, P., Cheng, J.X., Murre, C., Singh, H., Glass, C.K., 2010. Simple combinations of lineage-determining transcription factors prime cis-regulatory elements required for macrophage and B cell identities. Mol Cell 38, 576–589. doi:10.1016/j.molcel.2010.05.004

Kim, D., Pertea, G., Trapnell, C., Pimentel, H., Kelley, R., Salzberg, S.L., 2013. TopHat2: accurate alignment of transcriptomes in the presence of insertions, deletions and gene fusions. Genome Biol. 14, R36. doi:10.1186/gb-2013-14-4-r36

Love, M.I., Huber, W., Anders, S., 2014. Moderated estimation of fold change and dispersion for RNA-seq data with DESeq2. Genome Biol. 15, 550. doi:10.1186/s13059-014-0550-8

Ravens, S., Yu, C., Ye, T., Stierle, M., Tora, L., 2015. Tip60 complex binds to active Pol II promoters and a subset of enhancers and co-regulates the c-Myc network in mouse embryonic stem cells. Epigenetics & Chromatin 8, 45. doi:10.1186/s13072-015-0039-z

Saldanha, A.J., 2004. Java Treeview--extensible visualization of microarray data. Bioinformatics 20, 3246–3248. doi:10.1093/bioinformatics/bth349

Tripathi, S., Pohl, M.O., Zhou, Y., Rodriguez-Frandsen, A., Wang, G., Stein, D.A., Moulton, H.M., DeJesus, P., Che, J., Mulder, L.C.F., Yángüez, E., Andenmatten, D., Pache, L., Manicassamy, B., Albrecht, R.A., Gonzalez, M.G., Nguyen, Q., Brass, A., Elledge, S., White, M., Shapira, S., Hacohen, N., Karlas, A., Meyer, T.F., Shales, M., Gatorano, A., Johnson, J.R., Jang, G., Johnson, T., Verschueren, E., Sanders, D., Krogan, N., Shaw, M., König, R., Stertz, S., García-Sastre, A., Chanda, S.K., 2015. Meta- and Orthogonal Integration of Influenza ``OMICs"" Data Defines a Role for UBR4 in Virus Budding. Cell Host and Microbe 18, 723–735. doi:10.1016/j.chom.2015.11.002